Large-signal compact diode noise modelling strategies for non-autonomous RF nonlinear applications

F. Bonani, S. Donati Guerrieri, G. Ghione

Politecnico di Torino, Dipartimento di Elettronica,
Corso Duca degli Abruzzi 24, I-10129 Torino, Italy, Phone +39 011 564 4140

***Abstract*— We discuss system-oriented approaches to identify large-signal, cyclostationary compact noise models of RF pn diodes based on the modulation of small-signal, stationary noise expressions. Two modulation schemes are proposed and compared against a reference solution provided by physics-based large-signal noise simulations. The results point out that the most common modulation scheme exploited in the literature does not compare well with the reference solution, at least when the device is operated near the cutoff frequency.**

I. Introduction

The design and optimization of RF and microwave analog functional blocks such as mixers and frequency multipliers call for the development of accurate and reliable noise models for devices operating in forced nonlinear, quasi-periodic large-signal (LS) conditions. LS operation is affected by nonstationary fluctuations, whose statistical properties are described by cyclostationary stochastic processes. Those are characterized by correlated frequency components: time periodicity assures that such correlation occurs only between frequencies at the same distance from an harmonic of the noiseless steady-state, thus leading to the concept of noise sidebands [1], [2]. The correlation spectra between sidebands are collected into the Sideband Correlation Matrix (SCM) of the process, that characterizes the second-order statistical properties of cyclostationary fluctuations.

In LS noise modelling, many controversial points still remain: apart from the case of autonomous systems (oscillators), the development of accurate compact device models still requires investigations before satisfactory strategies can be implemented. Within this framework, physics-based (PB) simulations, derived from the numerical solution of a transport model rather than from approximate analytical approaches, make available a direct link between technology and the device noise behaviour, and thus (together with experimental characterization) can provide a reference for the development of physically sound compact models.

According to the literature, circuit-oriented compact cyclostationary noise models are commonly derived by the modulation, due to the time-varying device working point, of stationary compact models [3], [4]. The aim of this paper is to propose a comparison between two system-oriented modulation techniques applied to the determination of a pn diode LS noise compact model, and to validate the approaches against an accurate reference solution provided by physics-based large-signal noise simulations [2].

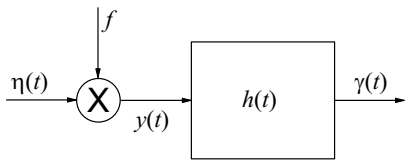

(a) Small-signal case

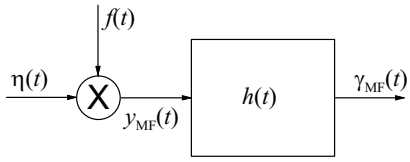

(b) Large-signal MF case

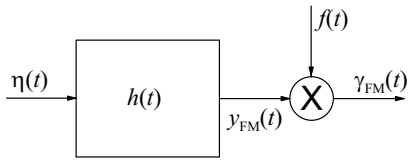

(c) Large-signal FM case

Fig. 1: Phenomenological approach to modulation: (a) system interpretation of stationary noise spectrum; (b) MF modulation scheme for cyclostationary noise model; (c) FM modulation scheme for cyclostationary noise model.

II. System-oriented modulation approaches

Since the seminal paper by Dragone [5] noise in LS conditions has been modelled, within the framework of compact device models, by assuming that small-signal (SS), stationary noise expressions are still valid as a base for cyclostationary noise extimation, the latter being founded on the assumption that the parts of the model dependent on the device working point are periodically modulated due to the LS device operation.

This approach leads to a unified interpretation of modulation if the stationary noise is white (as originally considered in [5], where shot noise in a diode was taken into account), while the case of colored small-signal noise spectra [4] is more involved. Let us interpret the stationary random process $\gamma(t)$ as described by the block diagram shown in Fig. 1 (a), i.e. the result of the multiplication of a unit white noise process $\eta(t)$ times a factor f dependent on the DC working point of the device, and filtered through a linear time-invariant system

with impulse response $h(t)$, describing the possibly colored nature of the spectrum. According to this picture, the power spectrum of the process $\gamma(t)$ is $S(\omega_{\rm ss}) = f^2|\tilde{h}(\omega_{\rm ss})|^2$, where $\tilde{h}(\omega)$ is the Fourier transform of $h(t)$.

Turning to LS conditions, the working point becomes periodically time varying so that f becomes a periodic function of time $f(t)$: this corresponds to an amplitude modulation of the stationary process, which is thus transformed into a cyclostationary random signal. According to the discussion in [6], modulation can be carried out in two ways: in the first case (Fig. 1 (b)), the amplitude modulation precedes the filtering stage (MF scheme). In the second scheme, amplitude modulation follows filtering (FM scheme). The two approaches lead to markedly different cyclostationary noise processes, since the SCM elements in the two cases are [6]:

$$\left(\mathbf{S}_{\rm MF}(\omega)\right)_{k,l} = \tilde{h}(\omega_k^+)(f^2)_{k-l}\tilde{h}^*(\omega_l^+), \tag{1}$$

$$\left(\mathbf{S}_{\rm FM}(\omega)\right)_{k,l} = \sum_{n=-\infty}^{+\infty} f_{k-n} f_{n-l} \left|\tilde{h}(\omega_n^+)\right|^2, \tag{2}$$

where $\omega_k^+ = \omega + k\omega_0$, ω is the sideband angular frequency, ω_0 is the angular frequency of the periodic steady-state, f_k is the k-th harmonic component (Fourier series coefficient) of the periodic function $f(t)$, and $(f^2)_k$ is the k-th harmonic component of the periodic function $f^2(t)$.

Both approaches lead to the same result in the case of white stationary noise, since this corresponds to $\tilde{h}(\omega) = 1$. On the other hand, if the small-signal spectrum is low-pass with cutoff frequency much lower than ω_0, (1) is always approximately zero except for the case $k = l = 0$ where:

$$\left(\mathbf{S}_{\rm MF}(\omega)\right)_{0,0} = \tilde{h}(\omega_0^+)(f^2)_0\tilde{h}^*(\omega_0^+), \tag{3}$$

while (2) reduces to:

$$\left(\mathbf{S}_{\rm FM}(\omega)\right)_{k,l} \approx f_k f_{-l} \left|\tilde{h}(\omega_0^+)\right|^2. \tag{4}$$

According to (4), FM gives rise to noise frequency conversion from baseband (assuming that the device is driven in nonlinear operation); on the other hand, MF does not provide this mechanism. As a general remark, the FM scheme is widely applied in the circuit modelling area [4], although in some cases the MF approach is also exploited [7], [8].

III. Diode modulated compact model

The MF and FM modulation schemes can be of course applied to the simulation of pn RF diodes. In small-signal conditions, if the device sides are short enough the current noise spectrum is given by the well-known shot expression, at least if forward bias only is considered:

$$S_I(\omega_{\rm ss}) = 2qI = 2qI_{\rm s}\left[\exp\left(\frac{V}{V_T}\right) - 1\right], \tag{5}$$

where I is the DC current, $I_{\rm s}$ is the junction reverse current, V is the junction voltage (excluding $R_{\rm s}$), and V_T is the thermal voltage. Application of (1) and (2) to this approximate expression yields, in LS conditions, the SCM originalli derived by Dragone [5]:

$$\left(\mathbf{S}_{\rm MF}(\omega)\right)_{k,l} = \left(\mathbf{S}_{\rm FM}(\omega)\right)_{k,l} = 2q(I)_{k-l}, \tag{6}$$

where $(I)_k$ is the k-th harmonic component of the LS time-varying current $I(t)$. Notice that this model applies only under the assumptions that (a) the LS device working point involves forward operation only, and (b) the maximum operating frequency (at the highest harmonic included in the model) is low enough to discard frequency dispersion effects in the small-signal noise spectrum.

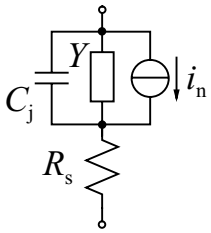

Fig. 2: Linearized diode equivalent circuit.

In the general case, a more complex expression for the device small-signal noise spectrum must be considered. A well known result [9], [10] yields:

$$\begin{aligned} S_I(\omega_{\rm SS}) &= 4k_{\rm B}T\mathrm{Re}\left\{Y(\omega_{\rm SS})\right\} - 2qI \\ &= 2q(I + 2I_{\rm s}) + 4k_{\rm B}T\left[\mathrm{Re}\left\{Y(\omega_{\rm SS})\right\} - Y(0)\right], \end{aligned} \tag{7}$$

where $k_{\rm B}$ is Boltzmann constant, T is the temperature, and $Y(\omega_{\rm SS})$ is the small-signal diode admittance due to the injection of minority carriers in the two neutral sides only. This means that the previous expression neglects both the effect of the parasitic series resistance $R_{\rm s}$ due to the majority carrier resistivity of the neutral sides, and of the junction (depletion) capacitance $C_{\rm j}(V)$ associated to the modulation of the depletion region width. In other words, (7) must be completed with the parasitic effects (embedding procedure) according to the equivalent circuit shown in Fig. 2.

Several degrees of approximation are possible for the explicit expression of (7), according to the approach exploited for evaluating the small-signal admittance $Y(\omega_{\rm SS})$: in the simplest case, a lumped model is used by describing $Y(\omega_{\rm SS})$ by means of the standard diffusion capacitance expression [11]. On the other hand, a more detailed analysis can be carried out leading to the so-called distributed model for the small-signal excess minority carrier concentrations [11]. For the distributed model, (7) is expressed as [12]:

$$\begin{aligned} S_I(\omega_{\rm SS}) = 2q^2A \sum_{\alpha=n,p} & \frac{D_\alpha/L_\alpha}{\cosh\left(2a_\alpha y_\alpha\right) - \cos\left(2b_\alpha y_\alpha\right)} \\ & \times \left\{g_\alpha\left[2a_\alpha \sinh\left(2a_\alpha y_\alpha\right) + 2b_\alpha \sin\left(2b_\alpha y_\alpha\right) - \coth(y_\alpha)\right.\right. \\ & \times \left.\left(\cosh\left(2a_\alpha y_\alpha\right) - \cos\left(2b_\alpha y_\alpha\right)\right)\right] \\ & \left.+2\alpha_{\overline{\alpha},\rm eq}\left[a_\alpha \sinh\left(2a_\alpha y_\alpha\right) + b_\alpha \sin\left(2b_\alpha y_\alpha\right)\right]\right\}, \end{aligned} \tag{8}$$

where $\overline{\alpha} = p, n$ for $\alpha = n, p$, A is the cross section, D_α, L_α are the diffusivity and the diffusion length of minority carrier α. Furthermore, $\alpha_{\overline{\alpha},\rm eq}$ is the equilibrium concentration of minority carriers in side $\overline{\alpha}$, while y_α is its physical length normalized to L_α. Functions $g_n = n_p'(-x_p)$ and $g_p = p_n'(x_n)$ represent the excess minority carrier concentrations at the border of the neutral regions, related to the applied voltage V through the junction law:

$$n_p'(-x_p) = n_{p,\rm eq}\left[\exp\left(\frac{V}{V_T}\right) - 1\right], \tag{9a}$$

$$p_n'(x_n) = p_{n,\rm eq}\left[\exp\left(\frac{V}{V_T}\right) - 1\right]. \tag{9b}$$

Finally, the frequency dependent part is given by the term $a_\alpha + \mathrm{j}b_\alpha = \sqrt{1+\mathrm{j}\omega_{\mathrm{ss}}\tau_\alpha}$, where τ_α is the minority carrier lifetime.

Application of (1) and (2) to (8) result into the modulated diode compact noise models. Notice that (8) contains an additive term independent of the working point, the part proportional to the equilibrium concentration of minority carriers in the two sides $\alpha_{\overline{\alpha},\mathrm{eq}}$, that would prevent the factorization required for applying the modulation schemes: for this reason, it will be neglected. Furthermore, the two noise contributions due to minority carriers in the two sides, being uncorrelated, can be modulated separately. According to this assumption, the noise spectrum contribution due to carrier α can be factorized as:

$$f_\alpha = \sqrt{2q^2 A \frac{D_\alpha}{L_\alpha} g_\alpha}, \tag{10}$$

$$\begin{aligned}\tilde{h}_\alpha(\omega_{\mathrm{SS}}) = &\{2a_\alpha \sinh(2a_\alpha y_\alpha) + 2b_\alpha \sin(2b_\alpha y_\alpha) \\ &- \coth(y_\alpha)\left[\cosh(2a_\alpha y_\alpha) - \cos(2b_\alpha y_\alpha)\right]\}^{1/2} \\ &\times \left[\cosh(2a_\alpha y_\alpha) - \cos(2b_\alpha y_\alpha)\right]^{-1/2}.\end{aligned} \tag{11}$$

Taking into account (10) and (11), (1) yields:

$$\begin{aligned}\left(\mathbf{S}_{\mathrm{MF}}(\omega)\right)_{k,m} = &\, 2q^2 A \sum_{\alpha=n,p} \frac{D_\alpha}{L_\alpha} (\tilde{g}_\alpha)_{k-m} \\ &\times \left\{2a^+_{\alpha,k} \sinh\left(2a^+_{\alpha,k} y_\alpha\right) + 2b^+_{\alpha,k} \sin\left(2b^+_{\alpha,k} y_\alpha\right)\right. \\ &\left. - \coth(y_\alpha)\left[\cosh\left(2a^+_{\alpha,k} y_\alpha\right) - \cos\left(2b^+_{\alpha,k} y_\alpha\right)\right]\right\}^{1/2} \\ &\times \left[\cosh\left(2a^+_{\alpha,k} y_\alpha\right) - \cos\left(2b^+_{\alpha,k} y_\alpha\right)\right]^{-1/2} \\ &\times \left\{2a^+_{\alpha,m} \sinh\left(2a^+_{\alpha,m} y_\alpha\right) + 2b^+_{\alpha,m} \sin\left(2b^+_{\alpha,m} y_\alpha\right)\right. \\ &\left. - \coth(y_\alpha)\left[\cosh\left(2a^+_{\alpha,m} y_\alpha\right) - \cos\left(2b^+_{\alpha,m} y_\alpha\right)\right]\right\}^{1/2} \\ &\times \left[\cosh\left(2a^+_{\alpha,m} y_\alpha\right) - \cos\left(2b^+_{\alpha,m} y_\alpha\right)\right]^{-1/2},\end{aligned} \tag{12}$$

while (2) gives the FM SCM:

$$\begin{aligned}\left(\mathbf{S}_{\mathrm{FM}}(\omega)\right)_{k,m} = &\, 2q^2 A \sum_l \sum_{\alpha=n,p} \frac{D_\alpha}{L_\alpha} (\tilde{g}_{\mathrm{sq},\alpha})_{k-l} (\tilde{g}_{\mathrm{sq},\alpha})^*_{l-m} \\ &\times \left\{2a^+_{\alpha,l} \sinh\left(2a^+_{\alpha,l} y_\alpha\right) + 2b^+_{\alpha,l} \sin\left(2b^+_{\alpha,l} y_\alpha\right)\right. \\ &\left. - \coth(y_\alpha)\left[\cosh\left(2a^+_{\alpha,l} y_\alpha\right) - \cos\left(2b^+_{\alpha,l} y_\alpha\right)\right]\right\} \\ &\times \left[\cosh\left(2a^+_{\alpha,l} y_\alpha\right) - \cos\left(2b^+_{\alpha,l} y_\alpha\right)\right]^{-1},\end{aligned} \tag{13}$$

where $(\tilde{g}_{\mathrm{sq},\alpha})_k$ is the k-th frequency component of $\sqrt{g_\alpha}$. In (12) and (13), we have defined $a^+_{\alpha,k} + \mathrm{j}b^+_{\alpha,k} = \sqrt{1+\mathrm{j}\omega^+_k \tau_\alpha}$.

IV. Results

To validate the compact models, we have simulated two Si abrupt pn junction, both with cross section normalized to 1 cm^2. The reference solution is provided, both for stationary and cyclostationary noise, by a numerical, 1D physics-based noise model [1], [2].

In the first case, we simulated a symmetric device with short (6 μm) sides and doping levels $N_{\mathrm{A}} = N_{\mathrm{D}} = 10^{16}$ cm^{-3}. The

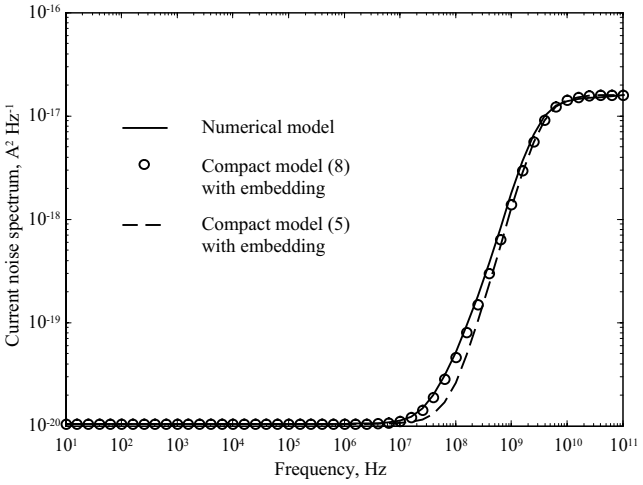

Fig. 3: Frequency dependence of the SS current noise spectrum for the short pn junction. Comparison among the reference solution (numerical model), the embedded compact model (5), and the embedded compact model (8).

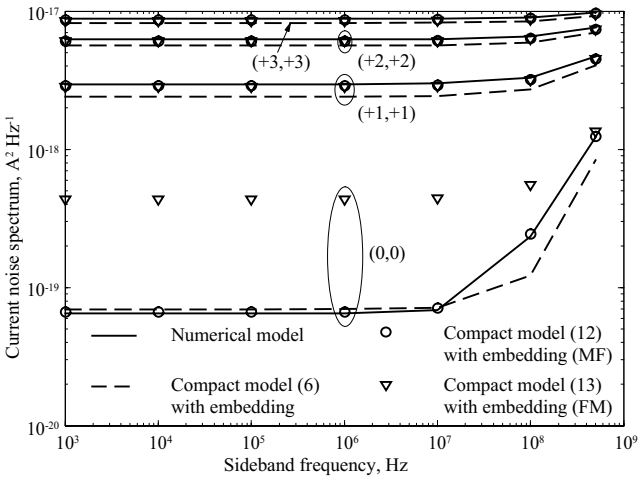

Fig. 4: Diagonal elements of the noise current SCM as a function of the sideband frequency for the short diode simulated for an input tone with amplitude 0.1 V at 1 GHz. Comparison among the reference solution (numerical model), the embedded compact model (6), the embedded MF compact model (12), and the embedded FM compact model (13).

minority carrier mobilities are $\mu_n = 1390$ cm^2 V^{-1} s^{-1} and $\mu_p = 470$ cm^2 V^{-1} s^{-1}, while minority carrier lifetimes are estimated as $\tau_n = \tau_p = 1$ μs. As a first comparison, we show in Fig. 3 the short-circuit current noise spectrum for a forward bias of 0.5 V as a function of frequency. In all the compact model results, the circuit elements not included in the model (i.e., the parasitic series resistance R_{s} and the junction capacitance C_{j}) have been taken into account in the comparison by means of a circuit embedding technique based on the equivalent circuit in Fig. 2. The series resistance has been estimated $R_{\mathrm{s}} = 1$ mΩ starting from the numerical SS device admittance, while the junction capacitance is evaluated according to the standard expression for abrupt junctions. According to Fig. 3, the distributed compact model (8) is in excellent agreement with the reference solution, but the simpler full shot noise model (5) is also in good agreement, since a discrepancy is observed only around the device corner frequency. Notice that for the pure shot model, the intrinsic

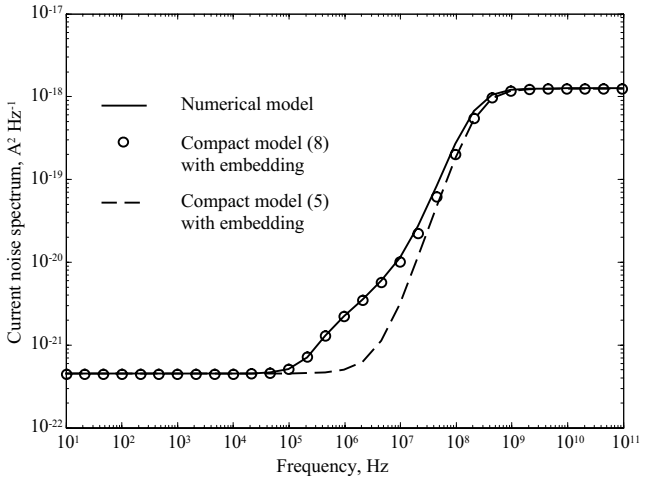

Fig. 5: Frequency dependence of the SS current noise spectrum for the n^+p junction. Comparison among the reference solution (numerical model), the embedded compact model (5), and the embedded compact model (8).

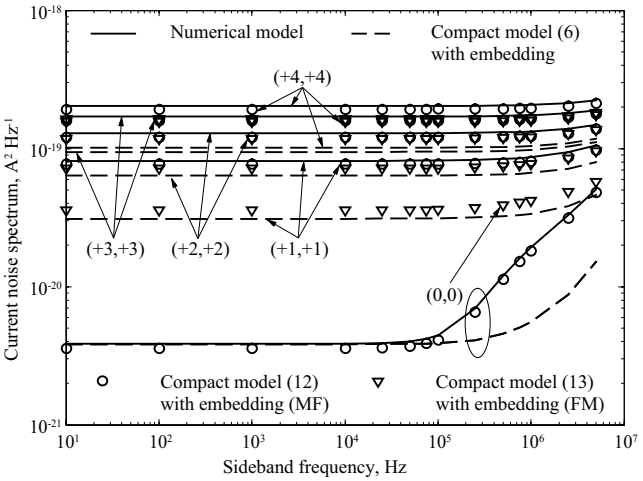

Fig. 6: Diagonal elements of the noise current SCM as a function of the sideband frequency for the n^+p diode simulated for an input tone with amplitude 0.1 V at 10 MHz. Comparison among the reference solution (numerical model), the embedded compact model (6), the embedded MF compact model (12), and the embedded FM compact model (13).

noise current spectrum is white, therefore the frequency dependence observed in the embedded spectrum is entirely due to a filtering effect corresponding to the reactive elements in the equivalent circuit of Fig. 2.

The same structure was then simulated in LS conditions, where the input signal is made of a one tone at 1 GHz with amplitude 0.1 V superimposed to a 0.5 V DC component. The numerical reference solution, obtained by solving the numerical physics-based model with the harmonic balance technique including 6 harmonics plus DC, is compared in Fig. 4 against the results of the embedded compact cyclostationary models discussed in Sec. III. We show the sideband frequency dependence of the available diagonal elements of the noise current SCM: according to the harmonics exploited for the working point determination, we show results up to the third sideband. The MF compact model (12) is in excellent agreement with the reference solution, while the FM model (13) strongly overestimates noise in the baseband sideband, although the error becomes significantly smaller for the upper sidebands. The simplest compact model (6), finally, compares fairly well with the reference solution for all sidebands, and can be therefore taken into consideration for this device.

In the second example, we simulated a n^+p structure, wherein the n^+ side, with doping $N_{\rm D} = 10^{18}$ cm^{-3}, is short (1 μm) and the p side is long (doping level $N_{\rm A} = 10^{16}$ cm^{-3}). Minority carrier mobilities are $\mu_n = 1250$ cm^2 V^{-1} s^{-1} and $\mu_p = 100$ cm^2 V^{-1} s^{-1}, while lifetimes are $\tau_n = 1$ ms and $\tau_p = 1$ μs. An SS simulation, is first carried out for a 0.5 V DC working point. The results are compared in Fig. 5 against the compact models (5) and (8). In both cases, the series resistance $R_{\rm s} = 13.3$ mΩ and the junction capacitance are embedded into the compact model results. The distributed noise spectrum based on (8) closely follows the theoretical estimation. The broken curve shows that in this case poor agreement results if the full shot noise (white) approximation is exploited, since a colored noise spectrum arises even for the intrinsic device.

Concerning cyclostationary noise, we have performed an LS simulation with a 0.1 V input tone at 10 MHz superimposed to the 0.5 V DC component, including 8 harmonics plus DC for the working point evaluation. The resulting noise current SCM diagonal elements are reported, as a function of the sideband frequency, in Fig. 6. The comparison is again carried out with the modulated compact models (6), (12) and (13), after embedding $R_{\rm s}$ and $C_{\rm j}$. In agreement with the behaviour observed for the short device (Fig. 4), the MF embedded compact model closely follows the reference solution, while the FM model significantly overestimates the baseband noise. A significant difference with the previous case is the disagreement observed for the simple compact model (6), observed for all sidebands except for the lowest frequencies in the baseband sideband $(0, 0)$.

REFERENCES

[1] F. Bonani, G. Ghione, *Noise in semiconductor devices. Modeling and simulation,* Springer Series in Advanced Microelectronics, Springer Verlag: Heidelberg, 2001.

[2] F. Bonani, S. Donati Guerrieri, G. Ghione, M. Pirola, "A TCAD approach to the physics-based modeling of frequency conversion and noise in semiconductor devices under large-signal forced operation", *IEEE Trans. El. Dev.*, Vol. ED-48, No. 5, pp. 966–977, May 2001.

[3] A. Demir, A. Sangiovanni-Vincentelli, *Analysis and simulation of noise in nonlinear electronic circuits and systems,* Kluwer Academic Publishers, Boston, 1998.

[4] V. Rizzoli, F. Mastri, D. Masotti, "General noise analysis of nonlinear microwave circuits by the piecewise Harmonic Balance technique," *IEEE Transactions on Microwave Theory and Techniques*, vol. 42, No. 5, pp. 807–819, May 1994.

[5] C. Dragone, "Analysis of thermal and shot noise in pumped resistive diodes,", *Bell Sys. Tech. J.,* vol. 47, pp. 1883–1902, 1968.

[6] F. Bonani, S. Donati Guerrieri, G. Ghione, "Noise source modeling for cyclostationary noise analysis in large-signal device operation", *IEEE Trans. El. Dev.*, Vol. ED-49, No. 9, pp. 1640–1647, September 2002.

[7] A. Demir, E. W. Y. Liu, A. Sangiovanni-Vincentelli, "Time-domain non Monte Carlo noise simulation for nonlinear dynamic circuits with arbitrary excitations," *IEEE Trans. on CAD*, Vol. 15, pp. 493–505, 1996.

[8] J. Roychowdhury, D. Long, P. Feldmann, "Cyclostationary noise analysis of large RF circuits with multitone excitations," *IEEE J. Solid-State Circuits*, vol. 33, no. 3, pp. 324–336, March 1998.

[9] K. M. van Vliet, "General transport theory of noise in *pn* junction-like devices – I: Three-dimensional Green's function formulation", *Solid State El.*, Vol. 15, pp. 1033–1053, 1972

[10] A. van der Ziel, *Noise in solid-state devices and circuits,* Wiley-Interscience: New York, 1986.

[11] S. M. Sze, *Physics of semiconductor devices,* John Wiley & Sons: New York, 2nd ed., 1981.

[12] F. Bonani, S. Donati Guerrieri, G. Ghione, "Compact conversion and cyclostationary noise modelling of pn junction diodes in low-injection — Part I: Model derivation", submitted to *IEEE Trans. El. Dev.*